

Design for a Time Variance - Gravitational Wave Detector (Version 3)

Peter CM Hahn
email: petehahn@telus.net
March 12, 2020

Abstract

This article describes a unique design for a device that will detect gravitational waves directly. The technique used in this design is based on the *inflow* that is predicted by foamy ether theory. Unlike current interferometer-based detectors that measure distortions of space caused by gravitational waves, the proposed Time Variance - Gravitational Wave Detector (TV-GWD) measures changes in the rate-of-flow-of-time.

The TV-GWD is capable of detecting much higher frequency signals than interferometer-based detectors because it measures fluctuations in time, instead of distortions in space. The TV-GWD can be mounted on a tabletop instead of requiring the kilometer-length antennas that are used by interferometers.

Details of the design and the tests performed are presented. Photos of an actual working prototype are also provided.

Keywords: gravitational waves, gravitational wave detector, general relativity, foamy ether theory

Table of Contents

INTRODUCTION	2
TV-GWD DESCRIPTION	3
LASER.....	3
OPTICS	3
PHOTO SENSORS.....	4
MODULE CONFIGURATION.....	6
TEST SIGNAL INJECTION SYSTEM DESCRIPTION	6
TEST RESULTS: DUAL PHOTODIODE ARRAY	7
TEST SIGNAL INJECTIONS	9
SETI TEST SIGNALS.....	10
CHIRP SIGNALS.....	11
TEST RESULTS: LINEAR ARRAY CAMERAS.....	13
DIGITAL ACQUISITION	14
TEST SIGNAL INJECTIONS	16
DETECTOR SENSITIVITY.....	18
DIFFRACTION ANGLE	18
SPECTRAL RESOLUTION.....	18
PLATE FACTOR	18
40MHZ CONFIGURATION SENSITIVITY.....	19
40KHZ CONFIGURATION SENSITIVITY	19

RADIO INTERFERENCE REDUCTION.....	20
DETECTOR DIRECTIONALITY.....	20
CONCLUSION	21
CURRENT TV-GWD PROTOTYPE PHOTOS	22
REFERENCES	23

Introduction

According to Einstein’s general theory of relativity, compact massive astronomical objects in motion will generate gravitational waves. These gravitational waves will cause distortions in the fabric of space-time that ripple outwards at the speed of light. A number of gravitational wave detectors such as LIGO [1] and VIRGO [2] are currently in operation. These detectors are based on a laser interferometer configuration that is designed to detect minute distortions in space.

This article proposes the unique and innovative design of a device that detects gravitational waves directly by measuring minute fluctuations in the rate-of-flow-of-time. The technique used in this design is based on the ether *inflow* [3] that is predicted by Foamy Ether Theory FET [4].

This new Time Variance - Gravitational Wave Detector design is based on the premise that incoming gravitational waves will cause a variation in the rate-of-flow-of-time. This variation is explained in detail on the FET site [5], which states that incoming gravitational waves will cause a variance in the downward flow of ether at the earth’s surface. This will result in a fluctuation in the rate-of-flow-of-time.

The TV-GWD is also based on the principle that the diffraction pattern generated by a monochromatic light source (laser), traveling through a multiple slit device (or diffraction grating), can be used to accurately measure the laser’s wavelength (see Figure 1). Any change in the rate-of-flow-of-time will also correspondingly cause a change in the laser’s frequency (and wavelength). This will cause the angle (θ_m) of reflected light to change. Sensors placed at the peaks of this pattern are able to detect minute changes in the reflection angle (θ_m), thereby sensing a change in the laser’s wavelength (see Figure 2). The resulting signals are sent to a Digital Acquisition System (DAQ) for real-time data capture and storage. Captured data can then be analyzed later by Digital Signal Processing software.

The configuration shown in Figure 2 is actually two detectors in one. The laser beam goes through a beam splitter that splits the beam into two equal paths, which then land on two different types of photo detection sensors. The first contains a dual photodiode array that has a frequency response of 40MHz, and the second is a 2048 pixel linear array camera with a frequency response of 40kHz.

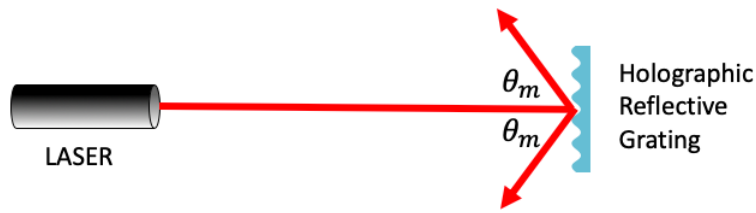


Figure 1 Reflective Diffraction Grating

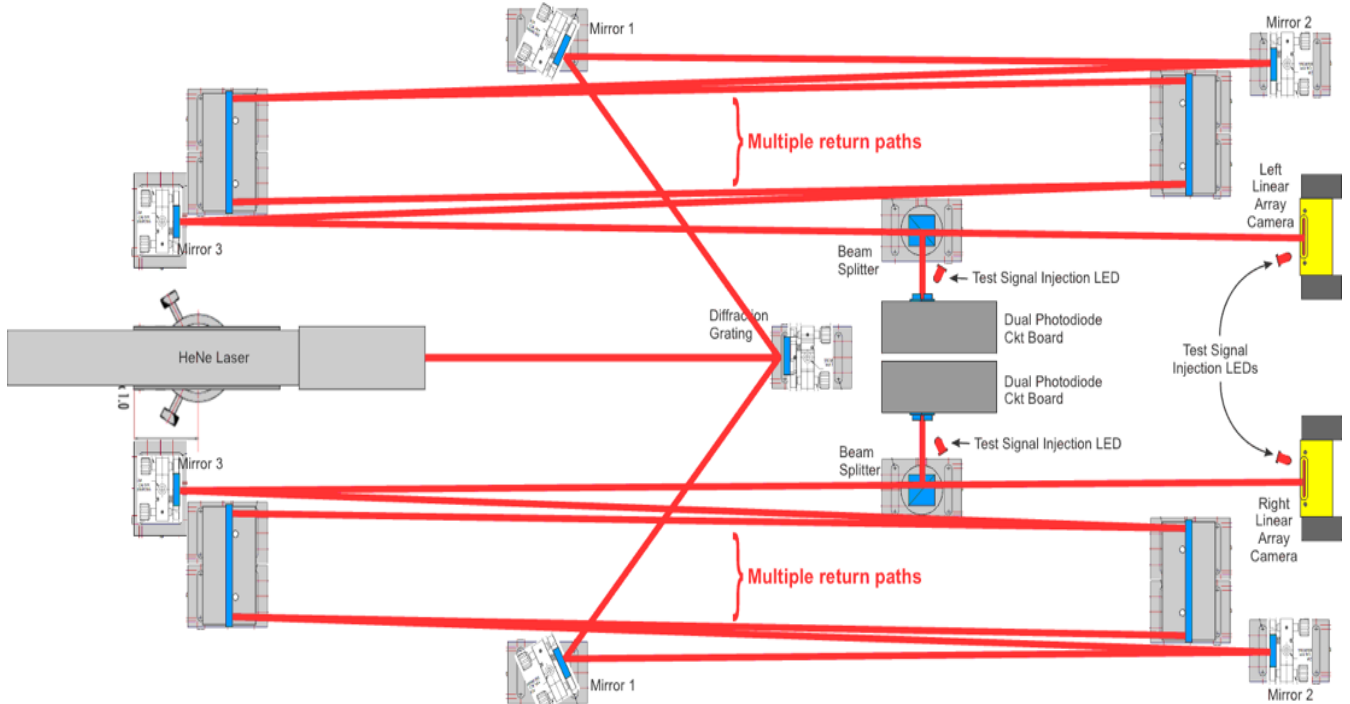


Figure 2 Optics Table

TV-GWD Description

Laser

A 2 mW Helium Neon (HeNe) laser [6] was chosen to generate a coherent, monochromatic light beam at a wavelength of 632.8 nm. The laser beam travels through a beam expander which maximizes the number of slits illuminated on the diffraction grating.

Optics

The HeNe laser is aimed at a holographic reflective diffraction grating that reflects the incident beam at a particular angle based on the laser's wavelength. The laser beam is reflected off multiple mirrors to maximize the distance traveled.

A 50/50 beam splitter is positioned at the tail end of the laser path such that half the beam lands on a dual set of photodiodes and half on a linear array camera.

Photo Sensors

The photodiode in use is an MTD5010W [7] which has an active collection area of one square mm. The laser beam lands on a pair of these photodiodes that are configured onto a light-balancing circuit (see Figure 3 and Figure 4). The light-balance circuit is designed to be sensitive only to the *difference* in light intensity of the two photodiodes so that any changes in the left and right position of the laser beam will produce an output signal. Since an increase in laser brightness will cause an equal increase in current output of both photodiodes, the light balance circuit configuration makes the receiver insensitive to laser intensity fluctuations.

Figure 3 shows a schematic diagram of the light balance circuit. The first stage operational amplifiers (opamps) (U1 & U2) convert the current from the two photodiodes (FD1 & FD2) into a voltage output signal. The second stage opamp (U3) is a differential amplifier that only produces a signal when the current from the two photodiodes differ. The laser beam is initially aligned so that there is no voltage present at the circuit output V_{out} . A gravitational wave passing through the detector will cause the rate-of-flow-of-time to fluctuate, thereby causing the frequency/wavelength of the laser to fluctuate. A change in wavelength will cause the light intensity at FD1 and FD2 to differ, thereby creating a voltage change at V_{out} .

Figure 5 is a plot of the frequency response of the light balance photodetector circuit. The brown line plots the frequency response of the first stage opamps U1 and U2. The green line plots the frequency response of final output V_{out} .

The output of the light balance circuit is sent to a high-speed analogue to digital converter via coaxial cable. The PCIE-1840L [8] in use has a 16-bit resolution, capable of capturing 4 channels simultaneously, at a rate of 80 mega samples per second (Msps). This makes the TV-GWD capable of detecting gravitational waves with a frequency as high as 40MHz.

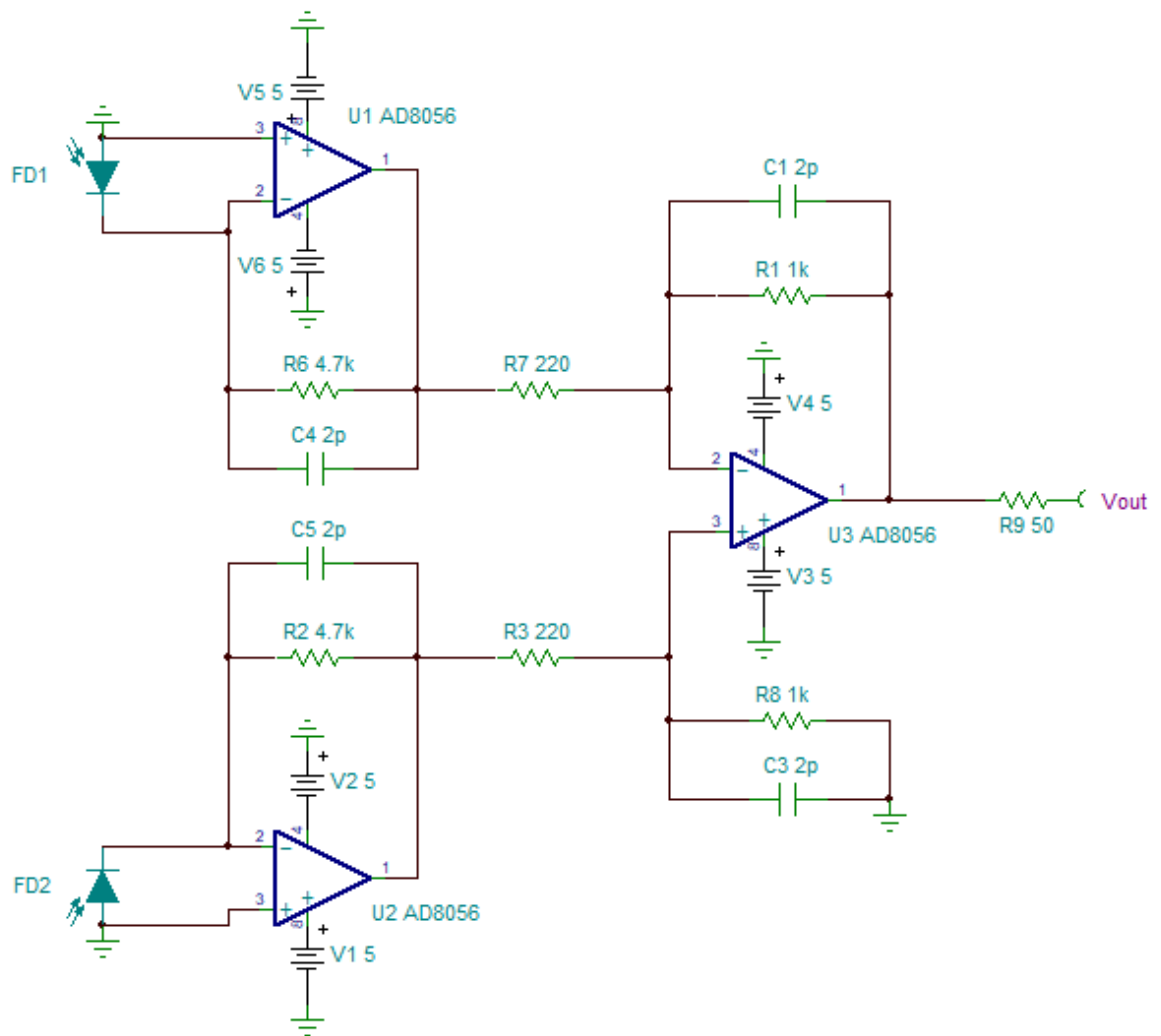


Figure 3 Light Balance Circuit

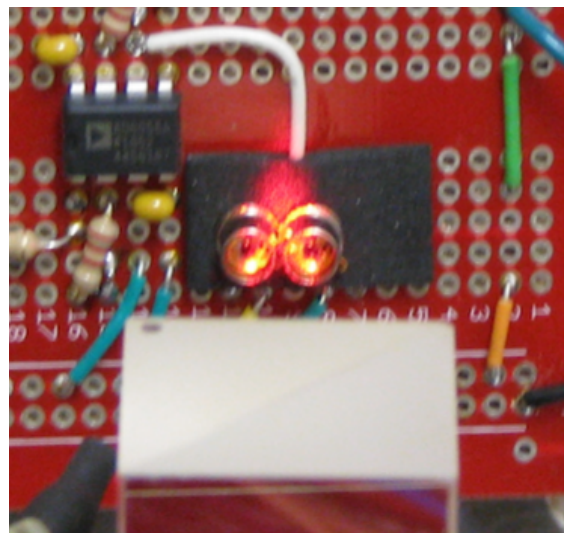


Figure 4 Dual Photodiodes

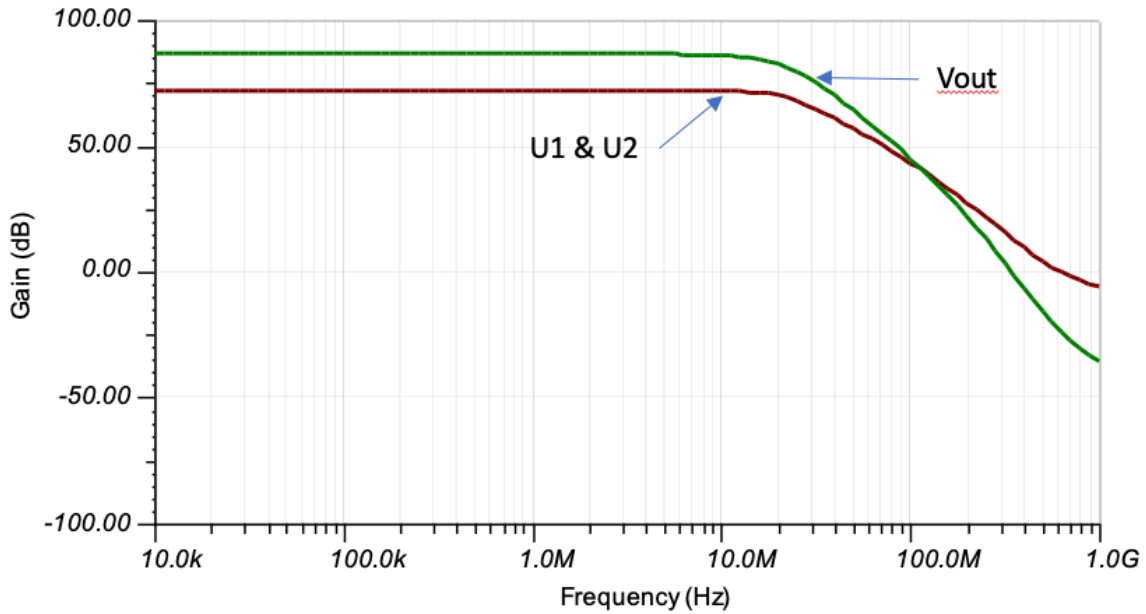


Figure 5 Frequency Response

Module Configuration

Figure 6 is a configuration diagram that shows the signal path from photodiode to data storage. The personal computer (PC) contains a PCIE-1840L expansion card that performs an analog-to-digital conversion of both the left and right signals at a rate of up to 80 Msps. The DAQNavI DataLogger application [9] is capable of displaying and logging the data to disk in real time. Various MATLAB [10] functions are then used for digital signal processing and analysis.

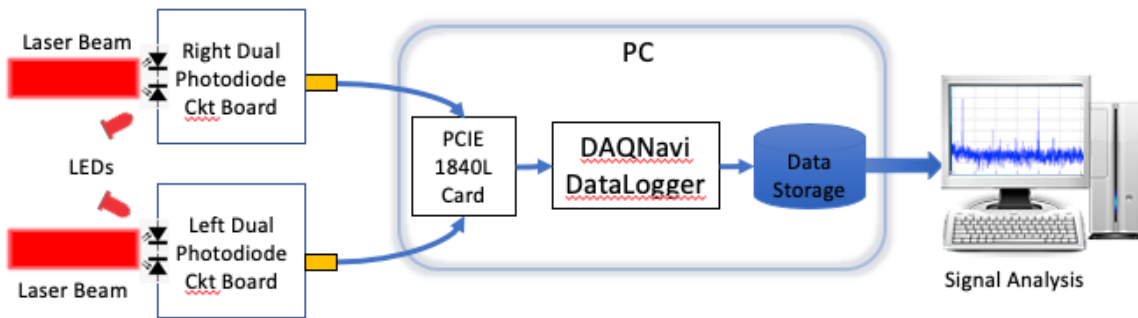


Figure 6 40MHz Configuration

Test Signal Injection System Description

Since there are currently no known methods of generating gravitational waves artificially, an alternate technique is required to mimic the effects a gravitational wave would have on the detector. LEDs are strategically placed in front and to the side of the dual photodiodes and the linear array cameras (see Figure 2). A test signal sent to these LEDs emulate the effect of the left and right movement of the laser beam that would normally result from a passing gravitational wave. A waveform generator [11] is used to inject various signal types into the LEDs to test the response parameters of the detector.

Test Results: Dual Photodiode Array

Figure 7 Time Domain Plot (no test signal injection) shows a typical time domain plot of a sample of data with no injected test signal present. The histogram in Figure 8 Histogram (no test signal injection) shows there is an obvious Gaussian distribution of noise caused by the HeNe laser and light-balance circuit.



Figure 7 Time Domain Plot (no test signal injection)

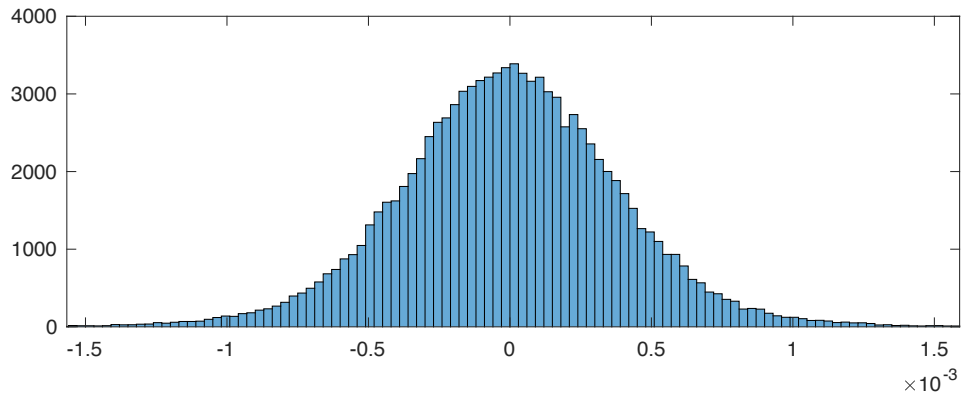


Figure 8 Histogram (no test signal injection)

Figure 9 is a frequency domain plot of a one second sample of data. MATLAB's pwelch function [12] plot shows a noticeable number of power spikes below 5MHz frequencies. These are caused by local radio interference (AM, FM, Ham, etc.).

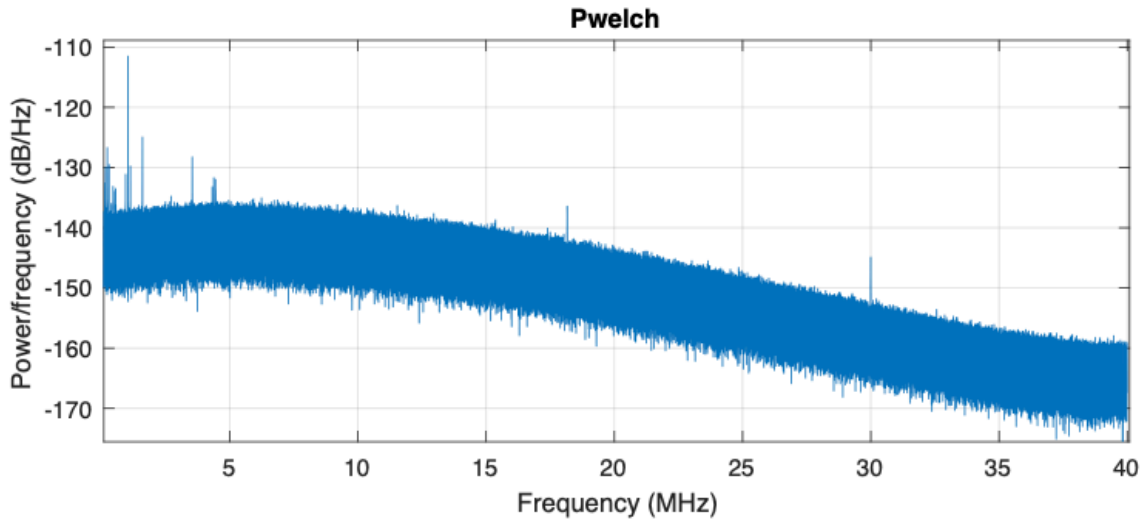


Figure 9 Power/Frequency – DC to 40MHz

A radio antenna connected to a RealTek software defined radio (RTL-SDR) receiver was used to generate a frequency scan of local radio stations (see Figure 11).



Figure 10 Radio Receiver

Figure 11 Power/Frequency Sweep – DC to 10MHz below is a power/frequency plot of local radio stations broadcasting at frequencies between DC and 10MHz.

Figure 12 Power/Frequency – DC to 10MHz is a plot of the power/frequency output of the TV-GWD which shows that most EM interference is attenuated because the light-balance circuit board is shielded by enclosing it in a metal box.

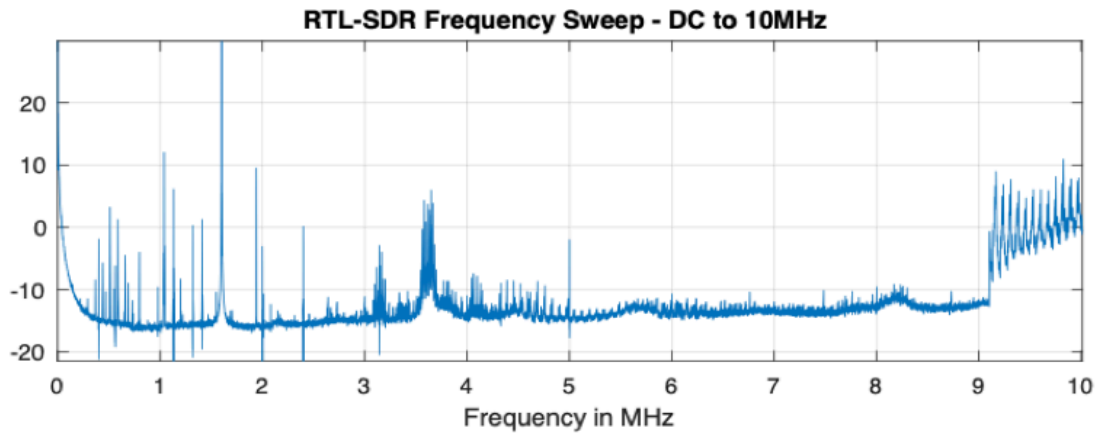


Figure 11 Power/Frequency Sweep – DC to 10MHz

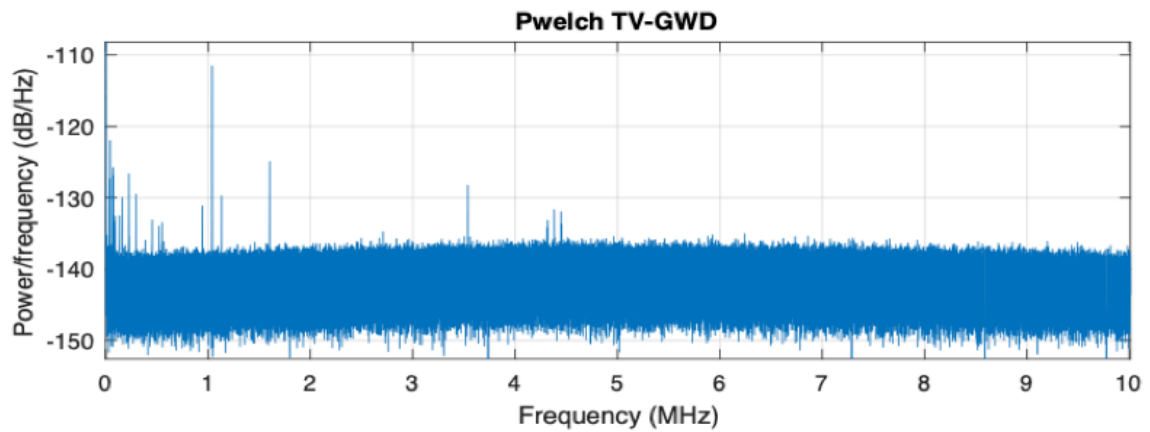


Figure 12 Power/Frequency – DC to 10MHz

Test Signal Injections

Various signals were injected into the system to test the frequency response of the TV-GWD. Figure 13 shows the results of the injection of 3MHz and 10MHz signals. The plot clearly displays the test signals and their respective harmonics of 6MHz and 20MHz.

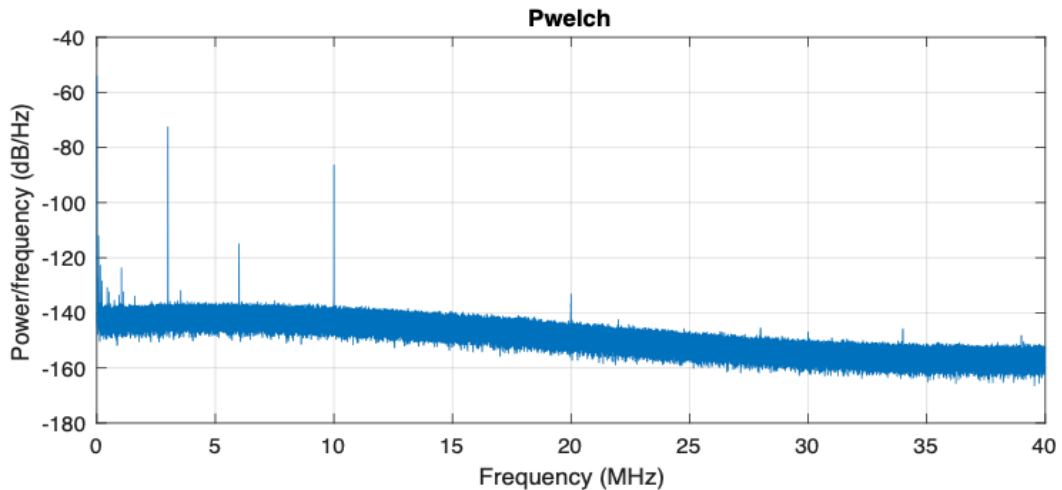


Figure 13 Power Levels of 3MHz and 10MHz Test Signals

SETI Test Signals

The TV-GWD is an ideal design for detecting gravitational waves that originate from intelligent, extraterrestrial sources, since it is sensitive to frequencies well into the megahertz range. (Current interferometer GW detectors are limited to frequencies in the few kilohertz range). GW waves have a significant advantage over EM waves for interstellar communication [13].

One of the signal types that the SETI team [14] is looking for are triplet pulses [15]. They are three power spikes that are equally spaced in time.

Figure 14 is a sample triplet pulse that was injected into the TV-GWD. The triplet is comprised of three 1MHz gaussian pulses, each separated by 4usec. Figure 15 is a CWT (Continuous Wavelet Transform) [16] plot of the triplet.

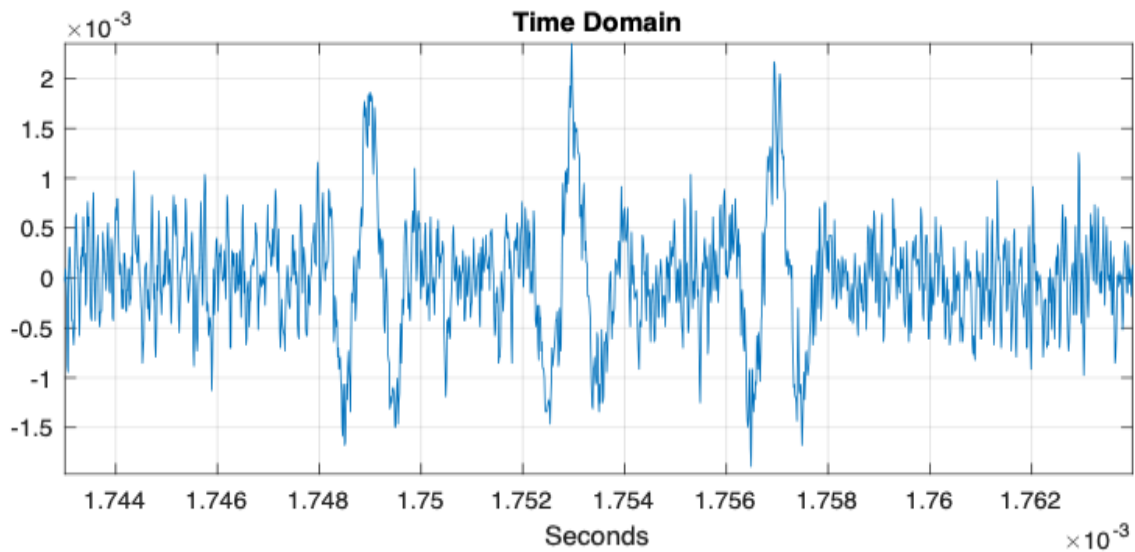


Figure 14 Time Domain Plot of a 1MHz Triple Pulse

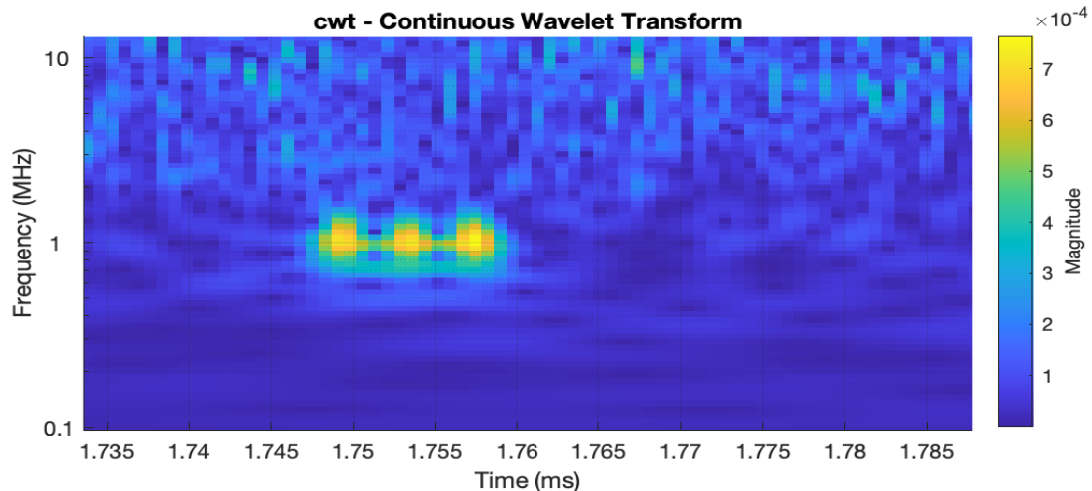


Figure 15 1MHz Triple Pulse

Figure 16 shows the time domain plot of a single 10MHz burst with a 2usec duration and Figure 17 shows its corresponding CWT.

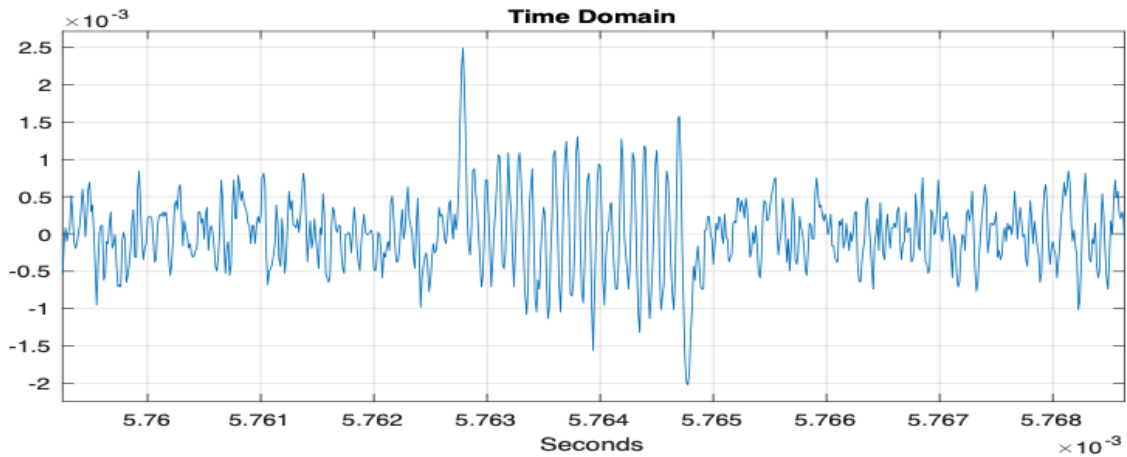


Figure 16 Time Domain Plot of 10MHz, 2usec Burst

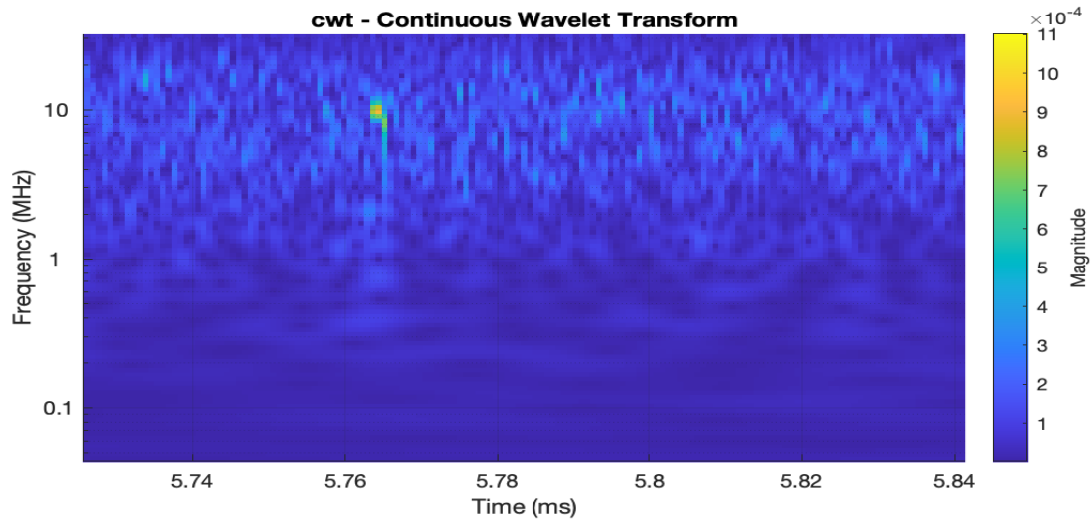


Figure 17 CWT - 10MHz, 2usec Burst

Chirp Signals

The TV-GWD can also be used to look for chirp signals that are indicative of a coalescence of two compact/dense objects, such as black holes or neutron stars. However, the TV-GWD can search megahertz frequencies that are currently out of range of detectors such as LIGO [1] and Virgo [2].

Figure 18 is a time domain plot of a test signal that simulates gravitational waves that may be produced by the coalescence of two dense objects. This signal was injected into the TV-GWD and Figure 19 is a plot of the data captured.

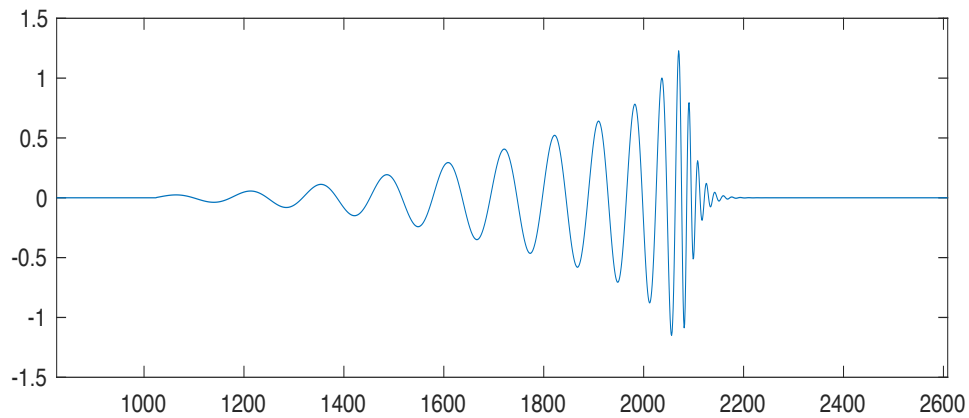


Figure 18 Chirp Test Injection Signal

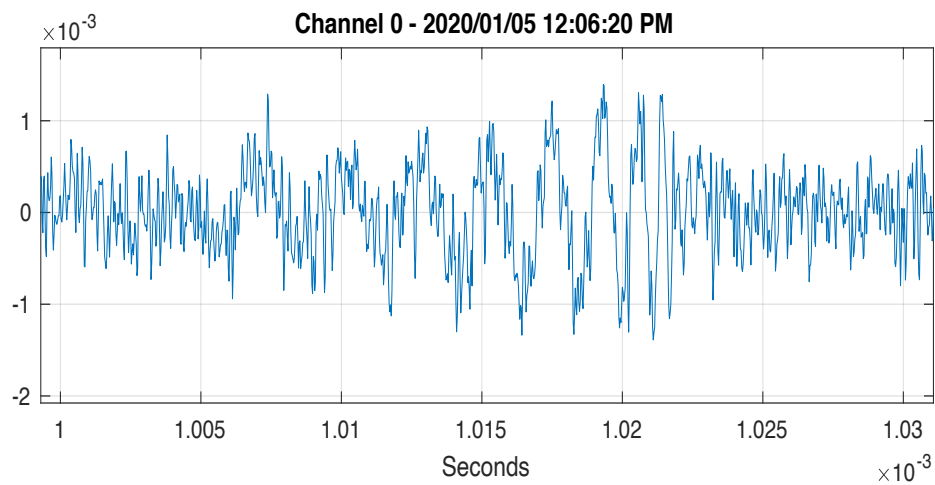


Figure 19 Time Domain Plot of Received Chirp Signal

Figure 20 is a spectrogram [17] of the signal that shows a 20usec chirp signal with a frequency sweep of 300kHz to 2.5MHz. Figure 21 shows a clearer picture of the chirp signal using a continuous wavelet transform [18].

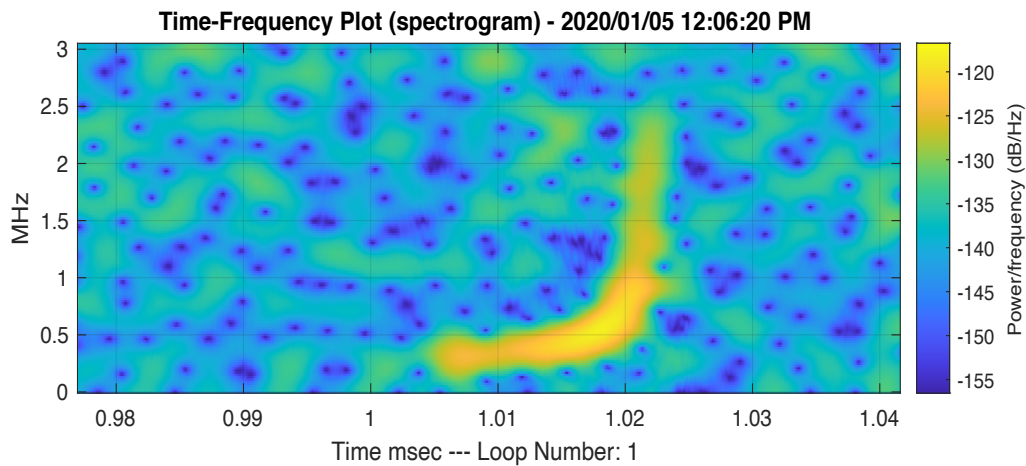


Figure 20 Spectrogram of Chirp Signal 300kHz to 2.5MHz

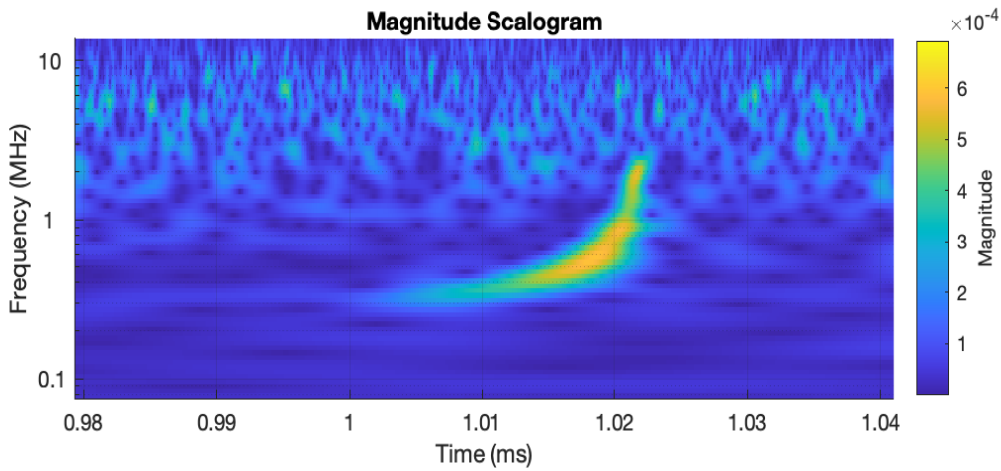


Figure 21 CWT of Chirp Signal 300kHz to 2.5MHz

Test Results: Linear Array Cameras

The configuration shown in Figure 22 was used to measure the sensitivity of the linear array cameras [19].

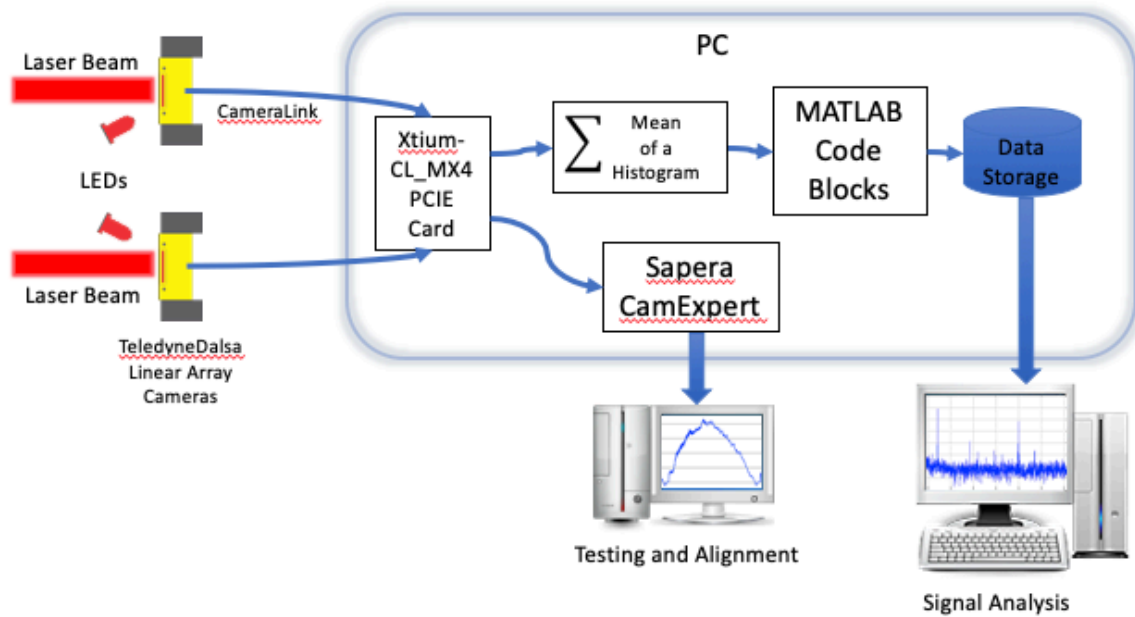


Figure 22 40kHz Configuration

Figure 23 and Figure 24 display plots of a typical frame captured by the left and right cameras respectively. The x-axis shows the pixel numbers of the linear array sensor (0 to 2047). The y-axis gives the 12-bit signal strength of each pixel (0 to 4095). The peaks and valleys show the etalon effect [20] caused by the transparent protective plate covering the CMOS sensors. Using Equation 1 for calculating the mean of a histogram, downstream processing calculates the center point (on the x-axis) of each frame and stores to disk. This center point is proportional to the wavelength of the laser. Any drift in the laser’s wavelength results in the image moving to the left or right, thereby changing the mean value.

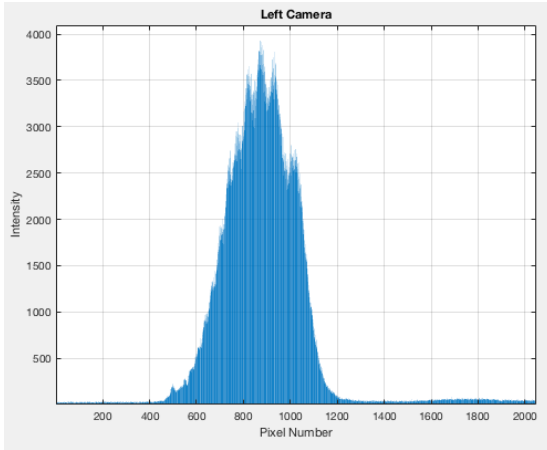


Figure 23 Left Camera

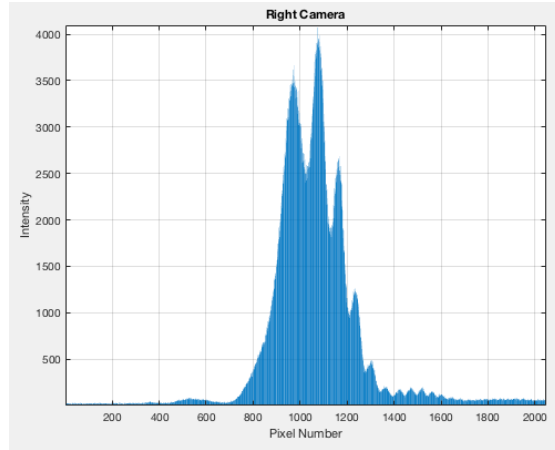


Figure 24 Right Camera

The equation for calculating the mean of a histogram is:

$$\mu = \frac{1}{N} \sum_{i=0}^{M-1} iH_i$$

Equation 1

Where:

N is the number of points in the signal

M is the number of points in the histogram

H_i are the values of the sampled signal

The corresponding C code for calculating the mean of a histogram is displayed in Figure 25. This configuration has the added benefit of making the detector insensitive to laser power fluctuations because the *horizontal position* of the mean is measured, not its amplitude.

```

mean = 0, n = 0;
for(int i=0; i<2048; i++){
    //read ADCportValue
    n = n + ADCportValue;
    mean = mean + i * ADCportValue;
}
mean = mean/n;

```

Figure 25 Mean of a Histogram

Digital Acquisition

The two linear array cameras capture the diffraction pattern at rate of 80,000 frames per second and send the data to an Xtium-CL MX4 frame grabber board [21]. The computer code shown in Figure 25 above calculates the mean of a histogram for each frame in real time and stores that data to disk.

Calculating the mean of the histogram is key to the operation of the detector. The varying frequency of the laser light causes the diffraction pattern to shift left and right on the linear array sensor, which in turn causes the mean of the histogram (for each frame) to vary as well. If the optical components are aligned properly, the peak of a node of the diffraction pattern will be centered on pixel number 1024 and the mean of the histogram will also be $2048/2$ or 1024.

Figure 26 Left and Right Signals shows a plot of approximately 4 minutes of a typical data capture where the blue line shows the data captured from the left camera and the orange line shows data from the right camera. The two signals are then added to eliminate any discrepancies between the two cameras which may be caused by unwanted seismic disturbances (see Figure 27 Left and Right Signals Added). The plot in Figure 27 Left and Right Signals Added also shows an additional low frequency drift that is caused by the instability of the laser. This low frequency drift is not a problem since it occurs over several seconds and downstream processing will ignore it.

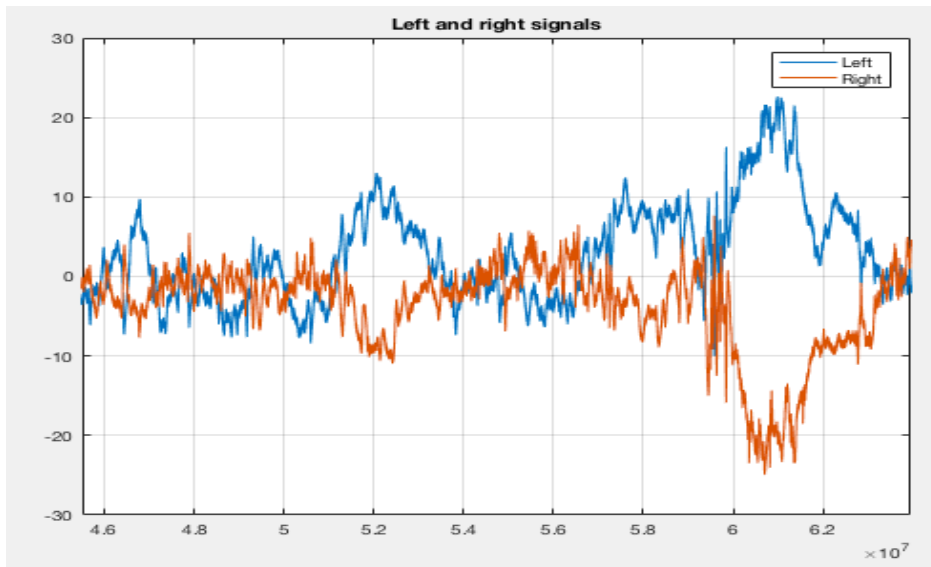


Figure 26 Left and Right Signals

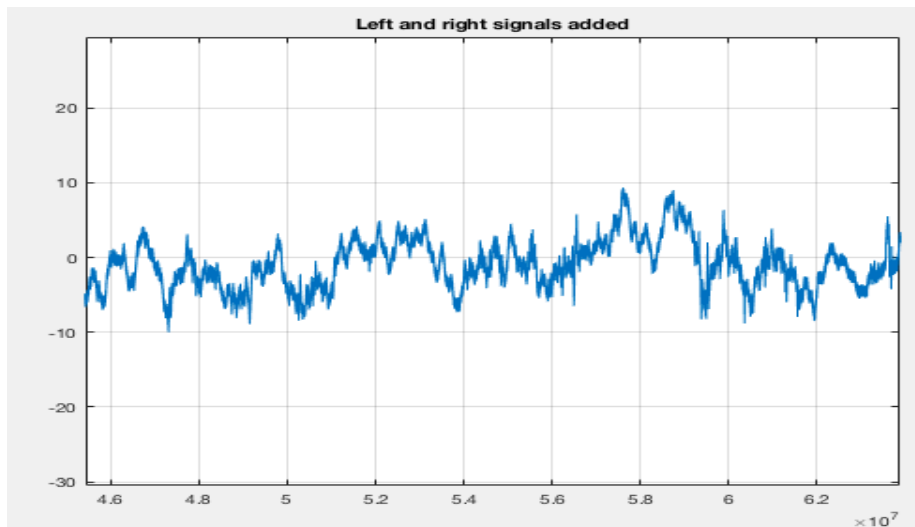


Figure 27 Left and Right Signals Added

Test Signal Injections

Test signal analysis described below was primarily achieved using MATLAB software. MATLAB's Signal Processing Toolbox [22] add-on software was also used to provide additional signal processing features.

Figure 28 shows a power spectral density plot of the data capture from Figure 27 Left and Right Signals Added. It reveals unexpected artifacts at 3.3kHz, 24.1kHz, 30.3kHz, 34.6kHz and 34.8kHz. Figure 29 reveals an *expected* 120Hz peak caused by the ripple noise from the power supply.

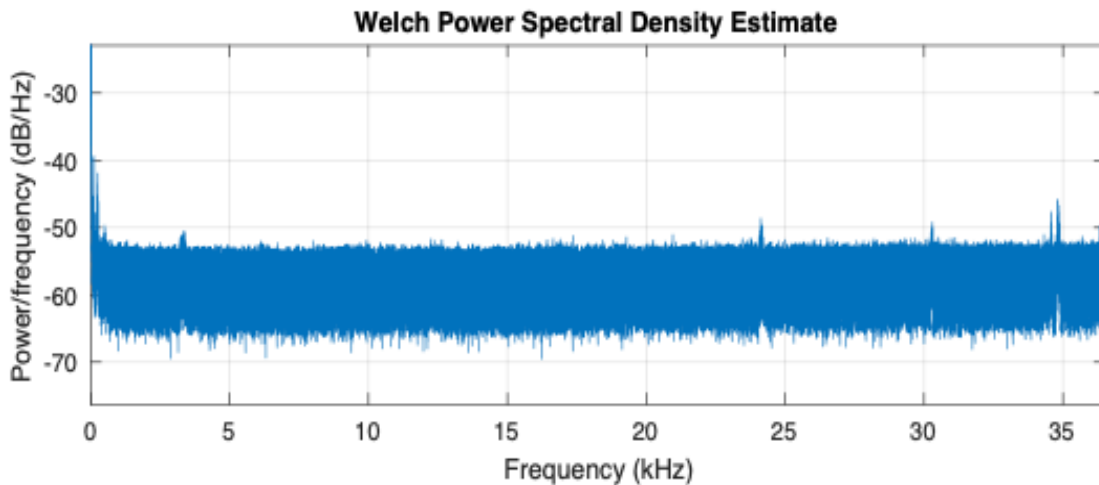


Figure 28 Unexpected Artifacts

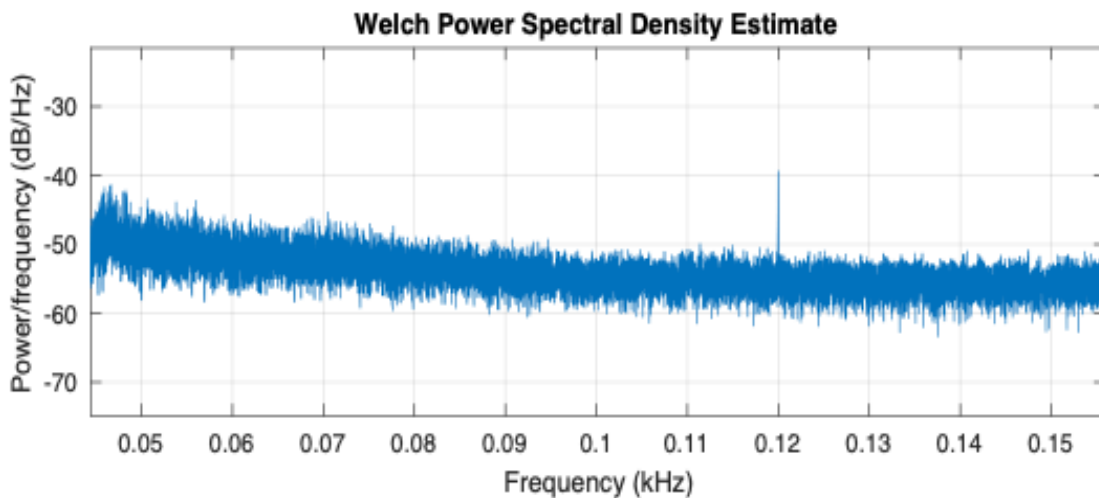


Figure 29 120Hz Power Supply Ripple

Figure 30 shows the results of a 30kHz sinusoidal test signal injected into the system for the duration of the capture, using an amplitude of 4mV peak to peak.

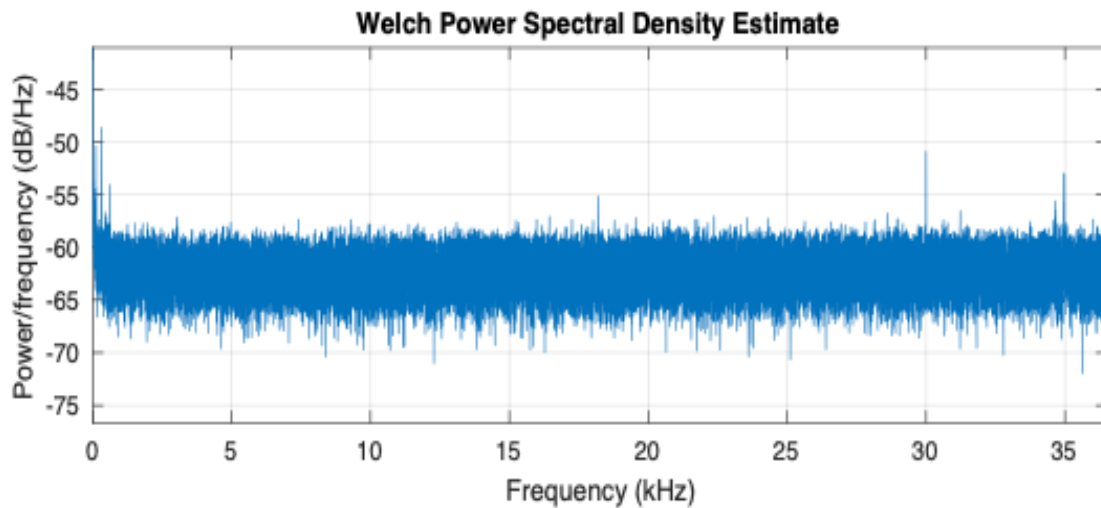


Figure 30 30kHz Test Signal

Figure 31 shows the time domain plot of a chirp signal injection (similar to Figure 18) sweeping from 2kHz to 25kHz with a duration of 4.5ms. This signal is similar to what a binary black hole merger would create (but at a higher frequency). Both the frequency and amplitude increase as the black holes merge, which is followed by an abrupt ringdown after the merger. The corresponding frequency/time domain plot (using a CWT) is illustrated in Figure 32.

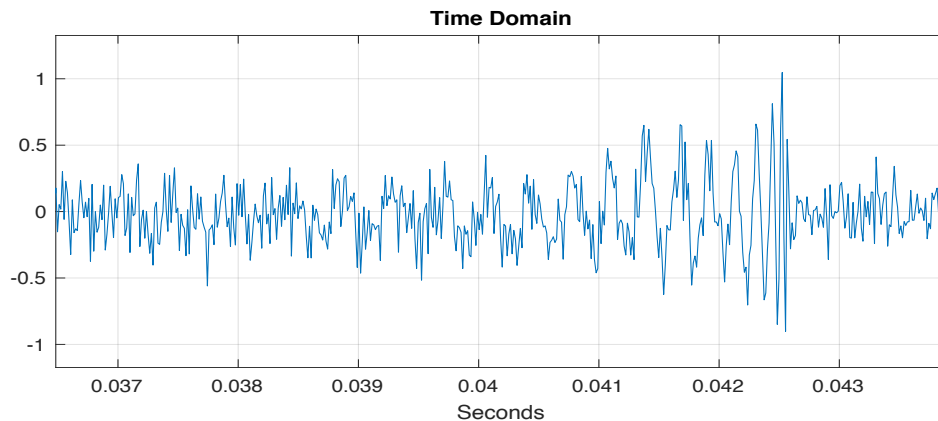


Figure 31 Chirp Signal – Time Domain

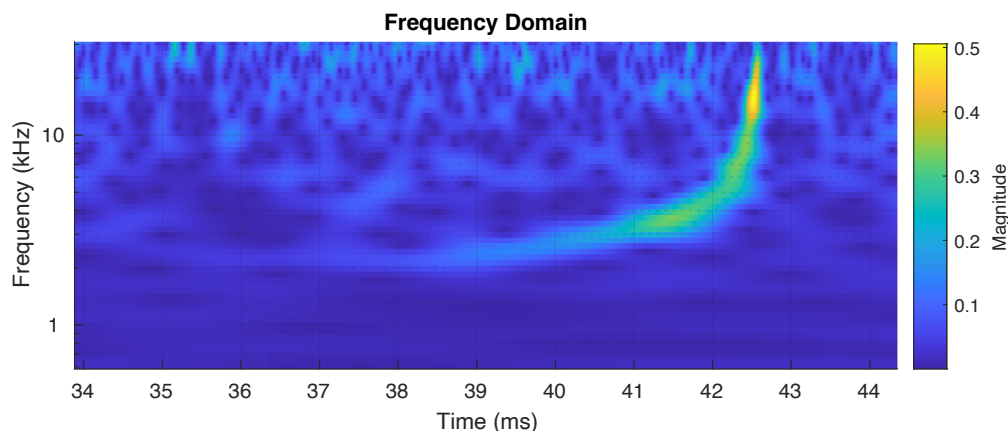


Figure 32 Chirp Signal – Frequency/Time Domain

Detector Sensitivity

Diffraction Angle

Referring to the layout in Figure 1, we can use the diffraction Equation 2 for calculating the angle of reflection.

$$\theta_m = \sin^{-1} \left(\sin \theta_i - \frac{m\lambda}{d} \right) \quad \text{Equation 2}$$

Where:

θ_m is the diffraction angle

θ_i is the angle of incidence

λ is the wavelength of the HeNe laser

m represents the propagation-mode (0,1,2,3...)

d is the distance between slits

The current TV-GWD detector uses a diffraction grating with 1200 slits/mm and a wavelength of 632.8nm, which results in a diffraction angle of 49.4078 degrees.

Spectral Resolution

The spectral resolution can be calculated using Equation 3 below.

$$\Delta\lambda = \frac{\lambda}{mN} \quad \text{Equation 3}$$

Where:

λ is the wavelength of the HeNe laser

m represents the propagation-mode (0,1,2,3...)

N is the number of slits that are illuminated on the diffraction grating

The HeNe laser is equipped with a 15X beam expander [23] that creates a beam that is 15mm in diameter. This allows for the illumination of 15 X 1200 slits, thereby resulting in a spectral resolution of 0.03516nm.

Plate Factor

The mirrors in Figure 2 are positioned in such a way that the laser beam reflects off the mirrors multiple times. This increases the effective distance the laser beam must travel. The current TV-GWD is configured for ten return paths, which increases the effective length of beam travel to approximately 19.57 meters. Equation 4 can be used to calculate the *plate factor* (P), which gives the sensitivity to change in wavelength in nm/mm.

$$P = \frac{d \cos \beta}{m \dot{r}}$$

Equation 4

Where:

d is the distance between slits

β is the reflected angle

m represents the propagation-mode (0,1,2,3...)

\dot{r} is the distance from the diffraction grating to the photodiode

In the configuration shown in Figure 2 Optics Table, the plate factor is calculated below.

$$P = 833\text{nm} \times \cos 49.4078 / (1 \times 19570) = 0.0277 \text{ nm/mm}$$

40MHz Configuration Sensitivity

For the configuration shown in Figure 6, the detector sensitivity $S_{\Delta t}$ can be calculated. Since the output of the two photodiodes is received by a 16 bit analogue-to-digital converter (ADC), a change in signal level of 2^{16} is attained. Therefore, the detector's sensitivity to the change in the rate-of-flow-of-time $\Delta t/t$ is limited by the plate factor and the output resolution of the ADC.

$$S_{\Delta t} = \frac{P}{N \lambda 2^{16}} = 0.0277\text{nm} / (2 \times 632.8\text{nm} \times 2^{16}) = 3.34 \times 10^{-10}$$

Where N = number of pixels in the array

40kHz Configuration Sensitivity

For the configuration shown in Figure 22, the detector sensitivity $S_{\Delta t}$ can also be calculated. The linear array cameras have 2048 pixels. Each pixel is converted to a digital value using a 12 bit ADC. A linear array camera substantially increases the detector's sensitivity, because the array now has 2048 photodiodes instead of just two. In this configuration, the detector's sensitivity to the change in the rate-of-flow-of-time $\Delta t/t$ is increased as calculated by the plate factor, the output resolution of the ADC and the number of pixels in the array.

$$S_{\Delta t} = \frac{P}{N \lambda 2^{12}} = 0.0277\text{nm} / (2048 \times 632.8\text{nm} \times 2^{12}) = 5.218 \times 10^{-12}$$

Radio Interference Reduction

Since the TV-GWD is sensitive well into the MHz range, it is likely that EM radio transmissions may cause interference. To reduce the likelihood that EM radiation will cause a false positive GW detection, the following configuration is proposed for future consideration. Figure 33 Simulink Blocks below shows MathWorks Simulink [24] blocks configured with an RTL-SDR receiver (first shown in Figure 10 Radio Receiver) to monitor and store radio signals in real time. Downstream processing can then compare these captured radio signals with stored signals from the TV-GWD (see Figure 6 and Figure 22 40kHz Configuration). If there is a match, it would be assumed that the signal is a result of radio interference, not a valid gravitational wave.

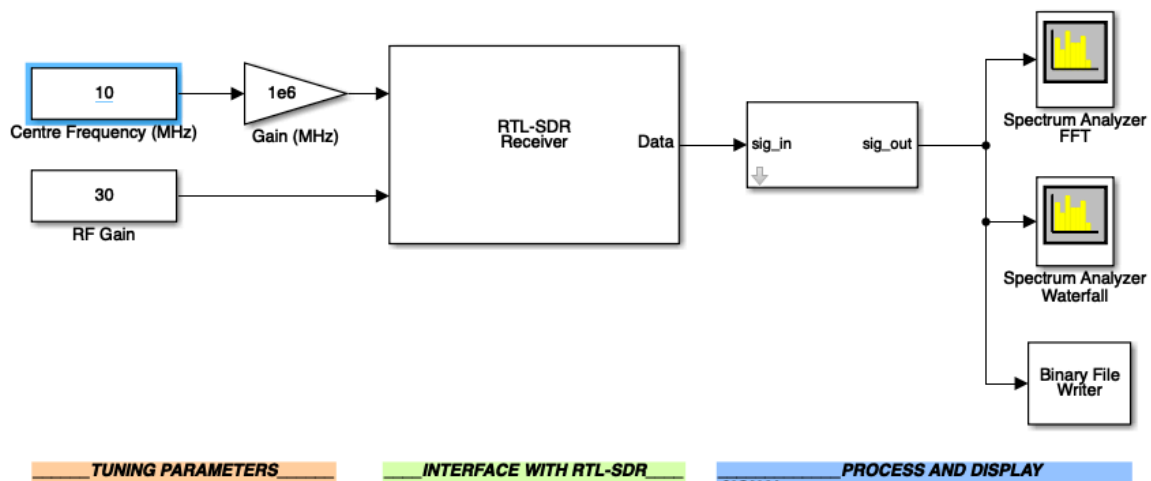


Figure 33 Simulink Blocks

Detector Directionality

A single TV-GWD is unable to determine the direction of the source signal since it only measures changes in the rate-of-flow-of-time. A three-dimensional array of at least four detectors would be required in order to determine the direction of the source gravitational wave. Detectors should be positioned at the vertices of a tetrahedron configuration.

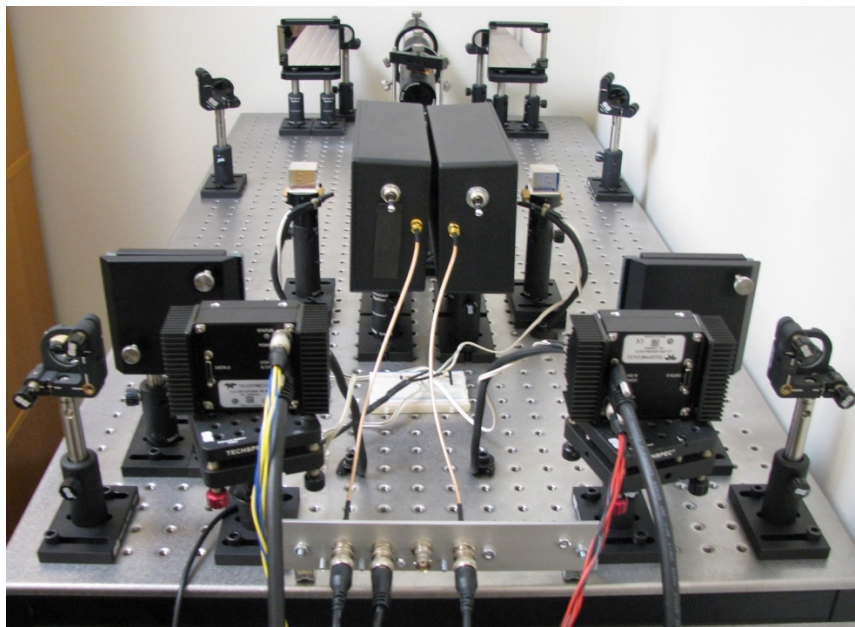
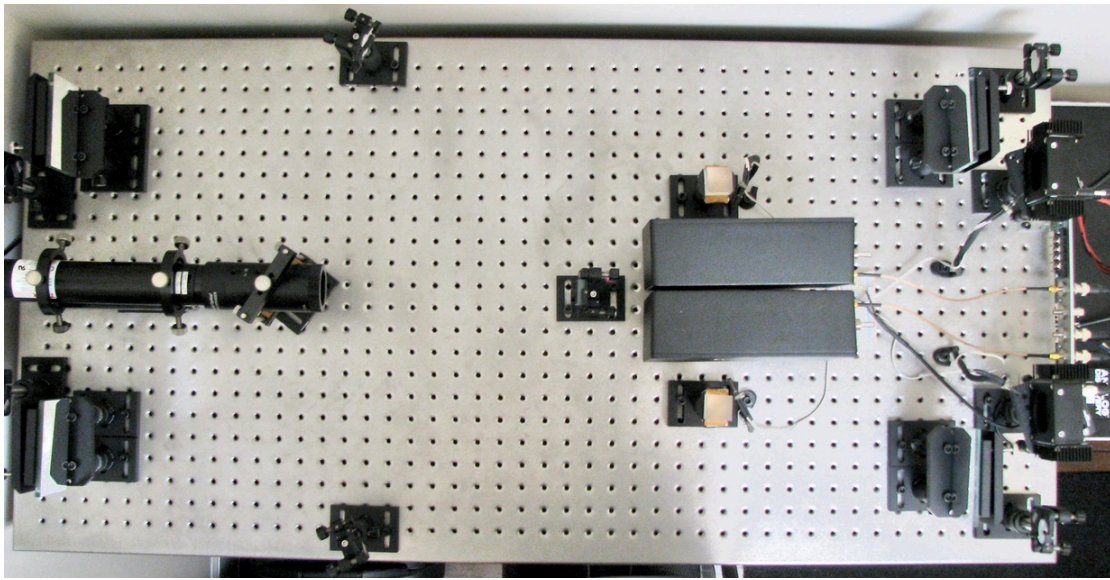
Conclusion

The TV-GWD offers an alternative design for a device that can be used to detect gravitational waves. Unlike current interferometer-based detectors that measure distortions of space caused by gravitational waves, the TV-GWD measures changes in the rate-of-flow-of-time. Because of this, the TV-GWD design allows for greater sensitivity in the higher frequency ranges that cannot be achieved by interferometer-based detectors. This also makes the TV-GWD an ideal device in the search for possible dark matter candidates such as coalescing primordial mini black holes [25].

The TV-GWD also has the ability to validate ether inflow that is predicted by foamy ether theory. However, a minimum of two detectors on opposite sides of the Earth would be required to confirm this theory. As predicted in foamy ether theory [26], gravitational waves entering one side of the planet will experience a 180 degree phase shift when leaving the opposite side.

In addition to analyzing gravitational waves originating from astrophysical sources, signals could also be analyzed for intelligent messages. Currently, projects such as seti@home [14] are looking for intelligent signals imbedded in electromagnetic waves. Advanced extraterrestrial civilizations may use gravitational waves as their preferred method of interstellar communication [13]. Intelligent signals would most likely be in the mega Hertz range which makes the high frequency capability of the TV-GWD an ideal device for detecting these signals.

Current TV-GWD Prototype Photos



References

- [1] LSC, "Laser Interferometer Gravitational-Wave Observatory," [Online]. Available: www.ligo.caltech.edu. [Accessed May 2020].
- [2] Virgo, "What is Virgo?," [Online]. Available: <http://www.virgo-gw.eu/#about>. [Accessed Jan 2020].
- [3] P. C. Hahn, "Gravity," [Online]. Available: <https://www.peterhahn.ca/gravity>. [Accessed Jan 2020].
- [4] P. C. Hahn, "Foamy (A)ether Theory - A Framework for a Theory Of Everything," [Online]. Available: <https://www.peterhahn.ca>. [Accessed Jan 2020].
- [5] P. C. Hahn, "Time Variance Gravitational Wave Detector," [Online]. Available: <https://www.peterhahn.ca/introduction-1>. [Accessed Jan 2020].
- [6] Thorlabs, "HeNe Lasers: Red," Thorlabs, [Online]. Available: https://www.thorlabs.com/newgrouppage9.cfm?objectgroup_id=1516. [Accessed Jan 2020].
- [7] Marktech, Marktech Optoelectronics, [Online]. Available: <https://marktechopto.com/marktech-detectors/silicon-photo-detectors/>. [Accessed Jan 2020].
- [8] Advantech, "Product Specification," Advantech, [Online]. Available: https://www.advantech.com/products/1-2mlk8i/pcie-1840/mod_a4a811bb-bc81-422f-a76e-15932ed6bc96. [Accessed Jan 2020].
- [9] Advantech, "DAQNavi Software Development Package for Advantech DAQ Products," Advantech, [Online]. Available: https://www.advantech.com/products/1-2mlcny/daqnavi/mod_82645e4e-0656-4592-ab56-c43902062d22. [Accessed Jan 2020].
- [10] MathWorks, "MATLAB Functions," MathWorks, [Online]. Available: https://www.mathworks.com/help/matlab/referencelist.html?type=function&istype=alpha&s_tid=CRUX_function. [Accessed Jan 2020].
- [11] Teledyne Lecroy, "WaveStation 2012," [Online]. Available: <https://www.digikey.ca/product-detail/en/teledyne-lecroy/WAVESTATION-2012/WAVESTATION2012-ND/3074037>. [Accessed Feb 2020].
- [12] MathWorks, "pwelch: Welch's power spectral density estimate," MathWorks, [Online]. Available: https://www.mathworks.com/help/signal/ref/pwelch.html?searchHighlight=pwelch&s_tid=doc_srchtile. [Accessed Jan 2020].
- [13] P. C. Hahn, "Search for Extraterrestrial Intelligence," [Online]. Available: <https://www.peterhahn.ca/seti>. [Accessed Jan 2020].
- [14] SETI@HOME, "What is SETI@HOME?," [Online]. Available: <https://setiathome.berkeley.edu>. [Accessed Jan 2020].
- [15] SETI@HOME, "SETI@home: Triplets," [Online]. Available: https://setiathome.berkeley.edu/sah_glossary/triplets.php. [Accessed Jan 2020].
- [16] MathWorks, "Continuous 1-D wavelet transform," MathWorks, [Online]. Available:

- https://www.mathworks.com/help/wavelet/ref/cwt.html?searchHighlight=cwt&s_tid=doc_srchtile. [Accessed Jan 2020].
- [17] MathWorks, "Spectrogram using short-time Fourier transform," MathWorks, [Online]. Available: https://www.mathworks.com/help/signal/ref/spectrogram.html?s_tid=doc_ta. [Accessed Jan 2020].
- [18] MathWorks, "Morse Wavelets," MathWorks, [Online]. Available: https://www.mathworks.com/help/wavelet/ug/morse-wavelets.html?searchHighlight=morse%20wavelet&s_tid=doc_srchtile. [Accessed Jan 2020].
- [19] T. Dalsa, "Linea," Teledyne Dalsa, [Online]. Available: <http://www.teledynedalsa.com/en/products/imaging/cameras/linea/>. [Accessed Jan 2020].
- [20] Wikipedia, "Fabry–Pérot interferometer," [Online]. Available: https://en.wikipedia.org/wiki/Fabry–Pérot_interferometer. [Accessed Jan 2020].
- [21] T. Dalsa, "Xtium CL MX4 Product Specification," [Online]. Available: <http://www.teledynedalsa.com/en/products/imaging/frame-grabbers/xtium-cl-mx4/>. [Accessed Feb 2020].
- [22] Mathworks, "Signal Processing Toolbox," [Online]. Available: <https://www.mathworks.com/products/signal.html>. [Accessed Feb 2020].
- [23] E. Optics, "15X Arcturus™ HeNe Beam Expander," Edmund Optics, [Online]. Available: <https://www.edmundoptics.com/p/15x-hene-fixed-beam-expander/15125/>. [Accessed Jan 2020].
- [24] MathWorks, "Simulation and Model-Based Design," [Online]. Available: https://www.mathworks.com/products/simulink.html?s_tid=hp_products_simulink. [Accessed Feb 2020].
- [25] J. K. S. S. W. X. Andrey Katz, "Looking for MACHOs in the Spectra of Fast Radio Bursts," 16 Dec. 2019. [Online]. Available: <https://arxiv.org/abs/1912.07620>.
- [26] P. C. Hahn, "Time Variance Gravitational Wave Detector: Ether Inflow," [Online]. Available: <https://www.peterhahn.ca/ether-inflow>. [Accessed Feb 2020].
- [27] LSC, "GraceDB — Gravitational-Wave Candidate Event Database," [Online]. Available: <https://gracedb.ligo.org/superevents/public/O3/>. [Accessed Jan 2020].